
Keeping Your Eye on the Ball: Trajectory Attention in Video Transformers

Mandela Patrick*

Facebook AI

mandelapatrick@fb.com

Dylan Campbell*

University of Oxford

dylan@robots.ox.ac.uk

Yuki Asano*

University of Oxford

yuki@robots.ox.ac.uk

Ishan Misra

Facebook AI

imisra@fb.com

Florian Metze

Facebook AI

fmetze@fb.com

Christoph Feichtenhofer

Facebook AI

feichtenhofer@fb.com

Andrea Vedaldi

Facebook AI

vedaldi@fb.com

João F. Henriques

University of Oxford

joao@robots.ox.ac.uk

Abstract

In video transformers, the time dimension is often treated in the same way as the two spatial dimensions. However, in a scene where objects or the camera may move, a physical point imaged at one location in frame t may be entirely unrelated to what is found at that location in frame $t + k$. These temporal correspondences should be modeled to facilitate learning about dynamic scenes. To this end, we propose a new drop-in block for video transformers—*trajectory attention*—that aggregates information along implicitly determined motion paths. We additionally propose a new method to address the quadratic dependence of computation and memory on the input size, which is particularly important for high resolution or long videos. While these ideas are useful in a range of settings, we apply them to the specific task of video action recognition with a transformer model and obtain state-of-the-art results on the Kinetics, Something-Something V2, and Epic-Kitchens datasets. Code and models are available at: <https://github.com/facebookresearch/Motionformer>.

1 Introduction

Transformers [76] have become a popular architecture across NLP [32], vision [20] and speech [4]. The self-attention mechanism in the transformer works well for different types of data and across domains. However, its generic nature and its lack of inductive biases also mean that transformers typically require extremely large amounts of data for training [57, 8], or aggressive domain-specific augmentations [72]. This is particularly true for video data, for which transformers are also applicable [51], but where statistical inefficiencies are exacerbated. While videos carry rich temporal information, they can also contain redundant spatial information from neighboring frames. Vanilla self-attention applied to videos compares pairs of image patches extracted at all possible spatial locations and frames. This can lead it to focus on the redundant spatial information rather than the temporal information, as we show by comparing normalization strategies in our experiments.

We therefore contribute a variant of self-attention, called *trajectory attention*, which is better able to characterize the temporal information contained in videos. For the analysis of still images,

* Equal contribution.

spatial locality is perhaps the most important inductive bias, motivating the design of convolutional networks [41] and the use of spatial encodings in vision transformers [20]. This is a direct consequence of the local structure of the physical world: points that belong to the same 3D object tend to project to pixels that are close to each other in the image. By studying the correlation of nearby pixels, we can thus learn about the objects.

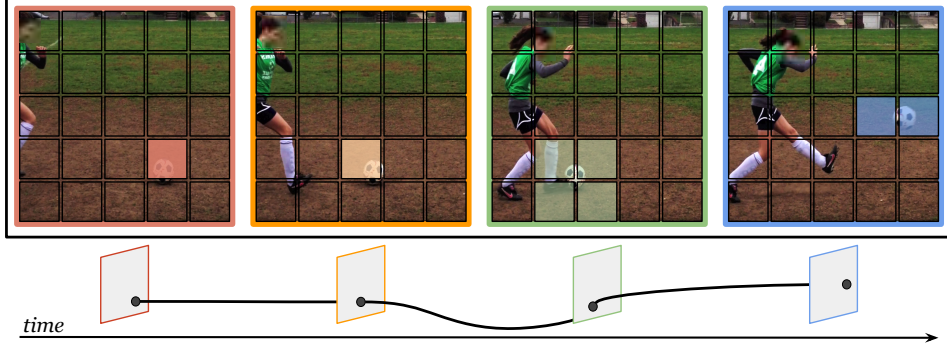


Figure 1: **Trajectory attention.** In this sequence of frames from the Kinetics-400 dataset, depicting the action ‘kicking soccer ball’, the ball does not remain stationary with respect to the camera, but instead moves to different locations in each frame. Trajectory attention aims to share information along the motion path of the ball, a more natural inductive bias for video data than pooling axially along the temporal dimension or over the entire space-time feature volume. This allows the network to aggregate information from multiple views of the ball, to reason about its motion characteristics, and to be less sensitive to camera motion.

Videos are similar, except that 3D points *move* over time, thus projecting on different parts of the image along certain 2D *trajectories*. Existing video transformer methods [7, 2, 51] disregard these trajectories, pooling information over the entire 3D space-time feature volume [2, 51], or pooling axially across the temporal dimension [7]. We contend that pooling along motion trajectories would provide a more natural inductive bias for video data, allowing the network to aggregate information from multiple views of the same object or region, to reason about how the object or region is moving (for example, the linear and angular velocities), and to be invariant to camera motion.

We leverage attention itself as a mechanism to find these trajectories. This is inspired by methods such as RAFT [71], which showed that excellent estimates of optical flow can be obtained from the correlation volume obtained by comparing local features across space and time. We observe that the joint attention mechanism for video transformers computes such a correlation volume as an intermediate result. However, subsequent processing collapses the volume without consideration for its particular structure. In this work, we seek instead to use the correlation volume to guide the network to pool information along motion paths.

We also note that visual transformers operate on image patches which, differently from individual pixels, cannot be assumed to correspond to individual 3D points and thus to move along simple 1D trajectories. For example, in Figure 1, depicting the action ‘kicking soccer ball’, the ball spans up to four patches, depending on the specific video frame. Furthermore, these patches contain a mix of foreground (the ball) and background objects, thus at least two distinct motions. Fortunately, we are not forced to select a single putative motion: the attention mechanism allows us to assemble a motion feature from all relevant ‘ball regions’.

Inspired by Nyströmformer [85], we also propose a principled approximation to self-attention, *Orthoformer*. Our approximation sets state-of-the-art performance on the recent Long Range Arena (LRA) benchmark [70] for evaluating efficient attention approximations and generalizes beyond the video domain to long text and high resolution images, with lower FLOPS and memory requirements compared to alternatives, Nyströmformer and Performer [14]. Combining our approximation with trajectory attention allows us to significantly improve its computational and memory efficiency. With our contributions, we set state-of-the-art results on four video action recognition benchmarks.

2 Related Work

Video representations and 3D-CNNs. Hand-crafted features were originally used to convert video data into a representation amenable to analysis by a shallow linear model. Such representations include SIFT-3D [61], HOG3D [38], and IDT [77]. Since the breakthrough of AlexNet [39] on the ImageNet classification benchmark [59], which demonstrated the empirical benefits of deep neural networks to learn representations end-to-end, there have been many attempts to do the same for video. Architectures with 3D convolutions—3D-CNNs—were originally proposed to learn deep video representations [73]. Since then, improvements to this paradigm include the use of ImageNet-inflated weights [10], the space-time decomposition of 3D convolutions [55, 75, 84], channel-separated convolutions [74], non-local blocks [80], and attention layers [12].

Vision transformers. The transformer architecture [76], originally proposed for natural language processing, has recently gained traction in the computer vision domain. The vision transformer (ViT) [20] decomposes an image into a sequence of 16×16 words and uses a multi-layer transformer to perform image classification. To improve ViT’s data efficiency, DeiT [72] used distillation from a strong teacher model and aggressive data augmentation. Transformers have also been used in a variety of vision image tasks, such as image representation learning [11, 83, 18, 60], image generation [52], object detection [47, 9], few-shot learning [19], and image-text representation learning [49, 63, 68, 43, 69], and video-text [65, 64, 87, 26, 54, 1, 5], and video-audio [42, 53, 29] representation learning. While the use of transformer architectures for video is still in its infancy, concurrent works [7, 2, 51, 22] have already demonstrated that this is a highly promising direction. However, these approaches do not have a mechanism for reasoning about motion paths, treating time as just another dimension, unlike our approach.

Efficient attention. Due to the quadratic complexity of self-attention, there has been a significant amount of research on how to reduce its computational complexity with respect to time and memory use. Sparse attention mechanisms [13] were used to reduce self-attention complexity to $\mathcal{O}(n\sqrt{n})$, and locality-sensitivity hashing was used by Reformer [37] to further reduce this to $\mathcal{O}(n \log n)$. More recently, linear attention mechanisms have been introduced, namely Longformer [6], Linformer [79], Performer [14] and Nyströmformer [85]. The Long Range Arena benchmark [70] was recently introduced to compare these different attention mechanisms.

Temporal correspondences and optical flow. There are many approaches that aim to establish explicit correspondences between video frames as a way to reason about camera and object motion. For short-range correspondences across time, optical flow algorithms [30, 66, 71] are highly effective. In particular, RAFT [71] showed the effectiveness of an all-pairs inter-frame correlation volume as an encoding, which is essentially an attention map. All-pairs intra-frame correlations were subsequently shown to help resolve correspondence ambiguities [34]. For longer-range correspondences, object tracking by repeated detection [58] and data association can be used. In contrast to these approaches, our work does not explicitly establish temporal correspondences, but facilitates implicit correspondence learning via trajectory attention. Jabri et al. [31] estimate correspondences in a similar way, framing the problem as a contrastive random walk on a graph and apply explicit guidance via a cycle consistency loss. Incorporating such guidance into a video transformer is an interesting direction.

3 Trajectory Attention for Video Data

Our goal is to modify the attention mechanism in transformers to better capture the information contained in videos. Consider an input video $I \in \mathbb{R}^{T' \times 3 \times H \times W}$ consisting of T' frames of resolution $H \times W$. As in existing video transformer models [7, 2], we pre-process the video into a sequence of ST tokens $\mathbf{x}_{st} \in \mathbb{R}^D$, for a spatial resolution of S and a temporal resolution of T . We use a cuboid embedding [2, 22], where disjoint spatio-temporal cubes from the input volume are linearly projected to \mathbb{R}^D (equivalent to a 3D convolution with downsampling). We also test an embedding of disjoint image patches [20]. A learnable positional encoding $\mathbf{e} \in \mathbb{R}^D$ is added to the video embeddings for spatial and temporal dimensions separately, resulting in the code $\mathbf{z}_{st} = \mathbf{x}_{st} + \mathbf{e}_s^s + \mathbf{e}_t^t$. Finally, a learnable classification token \mathbf{z}_{cls} is added to the sequence of tokens, like in the BERT Transformer [32], to reason about the video as a whole. For clarity, we elide the classification token from our treatment in the sequel.

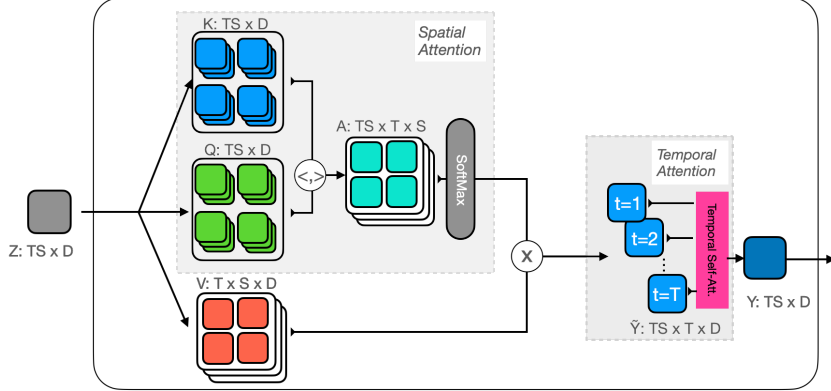


Figure 2: **Trajectory attention flowchart.** We divide the attention operation into two stages: the first forming a set of ST trajectory tokens for every space-time location st —a spatial attention operation between pairs of frames—and the second pooling along these trajectories with a 1D temporal attention operation. In this way, we accumulate information along the motion paths of objects in the video. The softmax operations are computed over the last dimension.

We now have a set of tokens that form the input to a sequence of transformer layers that, as in ViT [20], consist of Layer Norm (LN) operations [3], multi-head attention (MHA) [76], residual connections [28], and a feed-forward network (MLP):

$$\mathbf{y} = \text{MHA}(\text{LN}(\mathbf{z})) + \mathbf{z}; \quad \mathbf{z}' = \text{MLP}(\text{LN}(\mathbf{y})) + \mathbf{y}. \quad (1)$$

In the next section, we shall focus on a single head of the attention operation, and demonstrate how self-attention can realize a suitable inductive bias for video data. For clarity of exposition, we abuse the notation slightly, neglecting the layer norm operation and using the same dimensions for single-head attention as for multi-head attention.

3.1 Video self-attention

The self-attention operation begins by forming a set of query-key-value vectors $\mathbf{q}_{st}, \mathbf{k}_{st}, \mathbf{v}_{st} \in \mathbb{R}^D$, one for each space-time location st in the video. These are computed as linear projections of the input \mathbf{z}_{st} , that is, $\mathbf{q}_{st} = \mathbf{W}_q \mathbf{z}_{st}$, $\mathbf{k}_{st} = \mathbf{W}_k \mathbf{z}_{st}$, and $\mathbf{v}_{st} = \mathbf{W}_v \mathbf{z}_{st}$, for projection matrices $\mathbf{W}_i \in \mathbb{R}^{D \times D}$. A direct application of attention across space-time (called *joint space-time attention* [7, 2]) computes:

$$\mathbf{y}_{st} = \sum_{s't'} \mathbf{v}_{s't'} \cdot \frac{\exp\langle \mathbf{q}_{st}, \mathbf{k}_{s't'} \rangle}{\sum_{\bar{s}\bar{t}} \exp\langle \mathbf{q}_{st}, \mathbf{k}_{\bar{s}\bar{t}} \rangle}. \quad (2)$$

In this way, each query \mathbf{q}_{st} is compared to all keys $\mathbf{k}_{s't'}$ using dot products, the results are normalized using the softmax operator, and the weights thus obtained are used to average the values corresponding to the keys. Compared to a standard transformer, we have omitted for brevity the softmax temperature parameter $D^{1/2}$ and instead assume that the queries and keys have been divided by $D^{1/4}$.

One issue with this formulation is that it has quadratic complexity in both space and time, i.e., $\mathcal{O}(S^2T^2)$. An alternative is to restrict attention to either space or time (called *divided space-time attention*):

$$\mathbf{y}_{st} = \sum_{s'} \mathbf{v}_{s't} \cdot \frac{\exp\langle \mathbf{q}_{st}, \mathbf{k}_{s't} \rangle}{\sum_{\bar{s}} \exp\langle \mathbf{q}_{st}, \mathbf{k}_{\bar{s}t} \rangle} \text{ (space)}; \quad \mathbf{y}_{st} = \sum_{t'} \mathbf{v}_{st'} \cdot \frac{\exp\langle \mathbf{q}_{st}, \mathbf{k}_{st'} \rangle}{\sum_{\bar{t}} \exp\langle \mathbf{q}_{st}, \mathbf{k}_{s\bar{t}} \rangle} \text{ (time)}. \quad (3)$$

This reduces the complexity to $\mathcal{O}(S^2T)$ and $\mathcal{O}(ST^2)$, respectively, but only allows the model to analyse time and space independently. This is usually addressed by interleaving [7] or stacking [2] the two attention modules in a sequence.

Different to both of these approaches, we perform attention *along trajectories*. For each space-time location st (the trajectory ‘reference point’) and corresponding query \mathbf{q}_{st} , we construct a set of trajectory tokens $\tilde{\mathbf{y}}_{stt'}$. The trajectory extends for the duration of the video sequence and its tokens $\tilde{\mathbf{y}}_{stt'} \in \mathbb{R}^D$ at different times t' are given by:

$$\tilde{\mathbf{y}}_{stt'} = \sum_{s'} \mathbf{v}_{s't'} \cdot \frac{\exp\langle \mathbf{q}_{st}, \mathbf{k}_{s't'} \rangle}{\sum_s \exp\langle \mathbf{q}_{st}, \mathbf{k}_{s\bar{t}'} \rangle}. \quad (4)$$

Note that the attention in this formula is applied spatially (index s) and independently for each frame. Intuitively, this pooling operation implicitly seeks the location of the trajectory at time t' by comparing the trajectory query \mathbf{q}_{st} to the keys $\mathbf{k}_{s't'}$ at time t' .

Once the trajectories are computed, we further pool them across time. To do so, the trajectory tokens are projected to a new set of queries, keys and values as usual:

$$\tilde{\mathbf{q}}_{st} = \tilde{\mathbf{W}}_q \tilde{\mathbf{y}}_{stt}, \quad \tilde{\mathbf{k}}_{stt'} = \tilde{\mathbf{W}}_k \tilde{\mathbf{y}}_{stt'}, \quad \tilde{\mathbf{v}}_{stt'} = \tilde{\mathbf{W}}_v \tilde{\mathbf{y}}_{stt'}. \quad (5)$$

Like \mathbf{q}_{st} before, the updated reference query $\tilde{\mathbf{q}}_{st}$ corresponds to the trajectory reference point st and contains information spatially-pooled from across the reference frame t . This new query is used to pool across the new time (trajectory) dimension by applying 1D attention:

$$\mathbf{y}_{st} = \sum_{t'} \tilde{\mathbf{v}}_{stt'} \cdot \frac{\exp\langle \tilde{\mathbf{q}}_{st}, \tilde{\mathbf{k}}_{stt'} \rangle}{\sum_{\bar{t}} \exp\langle \tilde{\mathbf{q}}_{st}, \tilde{\mathbf{k}}_{st\bar{t}} \rangle}. \quad (6)$$

Like joint space-time attention, our approach has quadratic complexity in both space and time, $\mathcal{O}(S^2T^2)$, so has no computational advantage and is in fact slower than divided space-time attention. However, we demonstrate better accuracy than both joint and divided space-time attention mechanisms. We also provide fast approximations in Section 3.2. A flowchart of the full trajectory attention operation is shown in tensor form in Figure 2.

3.2 Approximating attention

To complement our trajectory attention, we also propose an approximation scheme to speed up calculations. This scheme is generic and applies to any attention-like pooling mechanism. We thus switch to a generic transformer-like notation to describe it. Namely, consider query-key-value matrices $\mathbf{Q}, \mathbf{K}, \mathbf{V} \in \mathbb{R}^{D \times N}$ such that the query-key-value vectors are stored as columns $\mathbf{q}_i, \mathbf{k}_i, \mathbf{v}_i \in \mathbb{R}^D$ in these matrices.

In order to obtain an efficient decomposition of the attention operator, we will rewrite it using a probabilistic formulation. Let $A_{ij} \in \{0, 1\}$ be a categorical random variable indicating whether the j th input (with key vector $\mathbf{k}_j \in \mathbb{R}^D$) is assigned to the i th output (with query vector $\mathbf{q}_i \in \mathbb{R}^D$), with $\sum_j A_{ij} = \mathbf{1}$. The attention operator uses a parametric model of the probability of this event based on the multinomial logistic function, i.e., the softmax operator $\mathcal{S}(\cdot)$:²

$$P(A_{i:}) = \mathcal{S}(\mathbf{q}_i^\top \mathbf{K}), \quad (7)$$

where the subscript $:$ denotes a full slice of the input tensor in that dimension. We now introduce the latent variables $U_{\ell j} \in \{0, 1\}$, which similarly indicate whether the j th input is assigned to the ℓ th *prototype*, an auxiliary vector which we denote by $\mathbf{p}_\ell \in \mathbb{R}^D$. We can use the laws of total and conditional probability to obtain:

$$P(A_{ij}) = \sum_{\ell} P(A_{ij} | U_{\ell j}) P(U_{\ell j}). \quad (8)$$

Note that the latent variables that we chose are independent of the inputs (keys). They use the same parametric model, but with parameters $\mathbf{P} \in \mathbb{R}^{D \times R}$ (the concatenated prototype vectors \mathbf{p}_ℓ): $P(U) = \mathcal{S}(\mathbf{P}^\top \mathbf{K})$. Eq. 8 is *exact*, even under the parametric model for $P(U)$, though the corresponding true distribution $P(A | U)$ is intractable. We now *approximate* the conditional probability $P(A | U)$ with a similar parametric model:

$$\tilde{P}(A | U) = \mathcal{S}(\mathbf{Q}^\top \mathbf{P}), \quad (9)$$

where $\mathbf{Q} \in \mathbb{R}^{D \times N}$ concatenates all query vectors horizontally. Substituting equations 7–9 we write the full approximate attention $\tilde{\mathcal{A}}$, multiplied by an arbitrary matrix \mathbf{V} (which in the case of a transformer contains the values of the key-value pairs stacked as rows):

$$\tilde{P}(A) \mathbf{V} = \mathcal{S}(\mathbf{Q}^\top \mathbf{P}) (\mathcal{S}(\mathbf{P}^\top \mathbf{K}) \mathbf{V}). \quad (10)$$

²I.e. $[\mathcal{S}(\mathbf{z})]_i = \exp(z_i / \sqrt{D}) / \sum_j \exp(z_j / \sqrt{D})$. For matrix inputs, the sum is over the columns.

Table 1: **Comparison of recent video transformer models.** We show the different design choices of recent video transformer models and how they compare to our proposed Motionformer model.

Model	Base Model	Attention	Pos. Encoding	Tokenization
TimeSformer [7]	ViT-B	Divided Space–Time	Separate	Square
ViViT [2]	ViT-L	Joint/Divided Space–Time	Joint	Cubic
Motionformer	ViT-B	Trajectory	Separate	Cubic

Computational efficiency. One important feature of the approximation in eq. 10 is that it can be computed in two steps. First the values \mathbf{V} are multiplied by a prototypes-keys attention matrix $\mathcal{S}(\mathbf{P}^\top \mathbf{K}) \in \mathbb{R}^{R \times N}$, which can be much smaller than the full attention matrix $\mathcal{S}(\mathbf{Q}^\top \mathbf{K}) \in \mathbb{R}^{N \times N}$ (eq. 7), i.e., $R \ll N$. Finally, this product is multiplied by a queries-prototypes attention matrix $\mathcal{S}(\mathbf{Q}^\top \mathbf{P}) \in \mathbb{R}^{N \times R}$, which is also small. This allows us to sidestep the quadratic dependency of full attention over the input and output size ($\mathcal{O}(N^2)$), replacing it with linear complexity ($\mathcal{O}(N)$) as long as R is kept constant.

Prototype selection. The aim for prototype-based attention approximation schemes is to use as few prototypes as possible while reconstructing the attention operation as accurately as possible. As such, it behooves us to select prototypes efficiently. We have two priorities for the prototypes: to dynamically adjust to the query and key vectors so that their region of space is well-reconstructed, and to minimize redundancy. The latter is important because the relative probability of a query–key pair may be over-estimated if many prototypes are clustered near that query and key. To address these criteria, we incrementally build a set of prototypes from the set of queries and keys such that a new prototype is maximally orthogonal to the prototypes already selected, starting with a query or key at random. This greedy strategy is dynamic, since it selects prototypes from the current set of queries and keys, and has high entropy, since it prefers well-separated prototypes. Moreover, it balances speed and performance by using a greedy strategy, rather than finding a globally-optimal solution to the maximum entropy sampling problem [62], making it suitable for use in a transformer.

Naïvely applying prototype-based attention approximation techniques to video transformers would involve creating a unique set of prototypes for each frame in the video. However, additional memory savings can be realized by sharing prototypes across time. Since there is significant information redundancy between frames, video data is opportune for compression via temporally-shared prototypes.

Orthoformer algorithm. The proposed approximation algorithm is outlined in Algorithm 1. The attention matrix is approximated using intermediate prototypes, selected as the most orthogonal subset of the queries and keys, given a desired number of prototypes R . To avoid a linear dependence on the sequence length N , we first randomly subsample cR queries and keys, for a constant c , before selecting the most orthogonal subset, resulting in a complexity quadratic in the number of prototypes $\mathcal{O}(R^2)$. The algorithm then computes two attention matrices, much smaller than the original problem, and multiplies them with the values. The most related approach in the literature is Nyströmformer [85] attention, outlined in Algorithm 2. This approach involves a pseudoinverse to attenuate the effect of near-parallel prototypes, has more operations, and a greater memory footprint.

Algorithm 1 Orthoformer (proposed) attention

- 1: $\mathbf{P} \leftarrow \text{MostOrthogonalSubset}(\mathbf{Q}, \mathbf{K}, R)$
- 2: $\Omega_1 = \mathcal{S}(\mathbf{Q}^\top \mathbf{P} / \sqrt{D})$
- 3: $\Omega_2 = \mathcal{S}(\mathbf{P}^\top \mathbf{K} / \sqrt{D})$
- 4: $\mathbf{Y} = \Omega_1(\Omega_2 \mathbf{V})$

Algorithm 2 Nyströmformer [85] attention

- 1: $\mathbf{P}_q, \mathbf{P}_k \leftarrow \text{SegmentMeans}(\mathbf{Q}, \mathbf{K}, R)$
- 2: $\Omega_1 = \mathcal{S}(\mathbf{Q}^\top \mathbf{P}_k / \sqrt{D})$
- 3: $\Omega_2^{-1} = \text{IterativeInverse}(\mathcal{S}(\mathbf{P}_q^\top \mathbf{P}_k / \sqrt{D}), N_{\text{iter}})$
- 4: $\Omega_3 = \mathcal{S}(\mathbf{P}_q^\top \mathbf{K} / \sqrt{D})$
- 5: $\mathbf{Y} = \Omega_1(\Omega_2^{-1}(\Omega_3 \mathbf{V}))$

3.3 The Motionformer model

Our full video transformer model builds on previous work, as shown in Table 1. In particular, we use the ViT image transformer model [20] as the base architecture, the separate space and time positional encodings of TimeSformer [7], and the cubic image tokenization strategy as in ViViT [2]. These design choices are ablated in Section 4. The crucial difference for our model is the trajectory attention mechanism, with which we demonstrate greater empirical performance than the other models.

Table 2: **Input encoding ablations:** Comparison of input tokenization and positional encoding design choices. We report GFLOPS and top-1 accuracy (%) on K-400 and SSv2.

(a) Cubic tokenization works best for trajectory attn.					(b) Trajectory attn. works well with both encodings.				
Attention	Tokenization	GFlops	K-400	SSv2	Attention	Pos. Encoding	GFlops	K-400	SSv2
Joint ST	Square (1×16^2)	179.7	79.4	63.0	Joint ST	Joint ST	180.6	79.1	60.8
	Cubic (2×16^2)	180.6	79.2	64.0		Separate ST [22]	180.6	79.2	64.0
Trajectory	Square (1×16^2)	368.5	79.4	65.8	Trajectory	Joint ST	369.5	79.6	65.8
	Cubic (2×16^2)	369.5	79.7	66.5		Separate ST [22]	369.5	79.7	66.5

4 Experiments

Datasets. **Kinetics** [35] is a large-scale video classification dataset consisting of short clips collected from YouTube, licensed by Google under Creative Commons. As it is a dataset of human actions, it potentially contains personally identifiable information such as faces, names and license plates. **Something-Something V2** [27] is a video dataset containing more than 200,000 videos across 174 classes, with a greater emphasis on short temporal clips. In contrast to Kinetics, the background and objects remain consistent across different classes, and therefore models have to reason about fine-grained motion signals. We verified the importance of temporal reasoning on this dataset by showing that a single frame model gets significantly worse results, a decrease of 39% top-1 accuracy. In contrast, a drop of only 7% is seen on the Kinetics-400 dataset, showing that temporal information is much less relevant there. We obtained a research license for this data from <https://20bn.com>; the data was collected with consent. **Epic Kitchens-100** [16] is an egocentric video dataset capturing daily kitchen activities. The highest scoring verb and action pair predicted by the network constitutes an action, for which we report top-1 accuracy. The data is licensed under Creative Commons and was collected with consent by the Epic Kitchens teams.

Implementation details. We follow a standard training and augmentation pipeline [2], as detailed in the appendix. For ablations, our default Motionformer model is the Vision Transformer Base architecture [20] (ViT/B), pretrained on ImageNet-21K [17], patch-size $2 \times 16 \times 16$ with central frame initialization [2], separate space-time positional embedding and our trajectory attention. The base architecture has 12 layers, 12 attention heads, and an embedding dimension of 768. For comparisons with state-of-the-art, we report results on two additional variants: Motionformer-HR, which has a high spatial resolution ($16 \times 336 \times 336$ videos), and Motionformer-L, which has a long temporal range ($32 \times 224 \times 224$ videos). Experiments with the large ViT architecture are deferred to the appendix.

4.1 Ablation studies

Input: tokenization. We consider the effect of different input tokenization approaches for both joint and trajectory attention on Kinetics-400 (K-400) and Something-Something V2 (SSv2) in Table 2b. For patch tokenization ($1 \times 16 \times 16$), we use inputs of size $8 \times 224 \times 224$, while for cubic [2, 22] tokenization ($2 \times 16 \times 16$), we use inputs of size $16 \times 224 \times 224$ to ensure that the model has the same number of input tokens over the same temporal range of 2 seconds. For both attention types, we see that cubic tokenization gives a 1% accuracy improvement over square tokenization on SSv2, a dataset for which temporal information is critical. Furthermore, our proposed trajectory attention using cubic tokenization outperforms joint space-time attention on both datasets.

Input: positional encoding. Here, we ablate using a joint or separate [22] (default) space-time positional encoding in Table 2b. Similar to the results for input tokenization, the choice of positional encoding is particularly important for the fine-grained motion dataset, SSv2. Since joint space-time attention treats tokens in the space-time volume equally, it benefits particularly from separating the positional encodings, allowing it to differentiate between space and time dimensions, with a 4% improvement on SSv2 over joint space-time encoding. Our proposed trajectory attention elicits a more modest improvement of 1% from using separated positional encodings on SSv2, and outperforms joint space-time attention in both settings on both datasets.

Attention block: comparisons. We compare our proposed trajectory attention to joint space-time attention [2], and divided space-time attention [7] in Table 4. Our trajectory attention (bottom row) outperforms both alternatives on the K-400 and SSv2 datasets. While we see only modest

Table 3: **Orthoformer ablations:** We ablate various aspects of our Orthoformer approximation. E denotes exact attention and A denotes approximate attention. We report max CUDA memory consumption (GB) and top-1 accuracy (%) on K-400 and SSv2.

(a) Orthoformer is competitive with Nyström.					(b) Selecting orthogonal prototypes is the best strategy.				
Attention	Approx.	Mem.	K-400	SSv2	Attention	Selection	Mem.	K-400	SSv2
Trajectory (E)	N/A	7.4	79.7	66.5	Trajectory (E)	N/A	7.4	79.7	66.5
Trajectory (A)	Performer	5.1	72.9	52.7	Trajectory (A)	Seg-Means	3.6	75.8	60.3
	Nyströmformer	3.8	77.5	64.0		Random	3.6	76.5	62.5
	Orthoformer	3.6	77.5	63.8		Orthogonal	3.6	77.5	63.8

(c) Approximation improves with more prototypes.					(d) Temporal sharing is the best strategy.				
Attention	# Prototypes	Mem.	K-400	SSv2	Attention	Sharing	Mem.	K-400	SSv2
Trajectory (E)	N/A	7.4	79.7	66.5	Trajectory (E)	N/A	7.4	79.7	66.5
Trajectory (A)	16	3.1	73.9	59.2	Trajectory (A)	✗	16.5	77.3	61.5
	64	3.3	74.9	63.0		✓	3.6	77.5	63.8
	128	3.6	77.5	63.8					

Table 4: **Attention ablations:** We compare trajectory attention with alternatives and ablate its design choices. We report GFLOPS and top-1 accuracy (%) on K-400 and SSv2. Att_T : temporal attention, Avg_T : temporal averaging, Norm_{ST} : space-time normalization, Norm_S : spatial normalization.

Attention	Att _T	Avg _T	Norm _S	Norm _{ST}	GFLOPS	K-400	SSv2
Joint Space-Time	–	–	–	–	180.6	79.2	64.0
Divided Space-Time	–	–	–	–	185.8	78.5	64.2
	✗	✓	✓	✗	180.6	76.0	60.0
	✓	✗	✗	✓	369.5	77.2	60.9
Trajectory	✓	✗	✓	✗	369.5	79.7	66.5

improvements on the appearance cue-reliant K-400 dataset, our trajectory attention significantly outperforms (+2%) the other approaches on the motion cue-reliant SSv2 dataset. This dataset requires fine-grained motion understanding, something explicitly singled out by previous video transformer works [2, 7] as a challenge for their models. In contrast, our trajectory attention excels on this dataset, indicating that its motion-based design is able to capture some of this information.

Attention block: trajectory attention design. We ablate two design choices for our trajectory attention: the per-frame softmax normalization and the 1D temporal attention. Unlike joint space-time attention, which normalizes the attention map over all tokens in space and time, trajectory attention normalizes independently per frame, allowing us to implicitly track the trajectories of query patches in time. In row 5 of Table 4, we ablate the benefits of this design choice. We observe a reduction of 2.5% on K-400 and 5.6% on SSv2 by normalizing over space and time (Norm_{ST}) compared with normalizing over space alone (Norm_S). In row 4, we show the benefit of using 1D temporal attention (Att_T) to aggregate temporal features, compared to average pooling (Avg_T). We observe reductions of 3.7% on K-400 and 6.5% on SSv2 when using average pooling instead of temporal attention applied to the motion trajectories, although it saves computing the additional query/key/value projections.

4.2 Orthoformer approximated attention

Approximation comparisons. In Table 3a, we compare our Orthoformer algorithm to alternative strategies: Nyströmformer [85] and Performer [14]. Our algorithm performs comparably with Nyströmformer with a reduced memory footprint. In Table 5, we also compare these attention mechanisms on the Long Range Arena benchmark [70] to show applicability to other tasks and data types. Orthoformer is able to effectively approximate self-attention, outperforming the state-of-the-art despite using far fewer prototypes (64) and so gaining significant computational and memory benefits.

Prototype selection. A key part of our Orthoformer algorithm is the prototype selection procedure. In Table 3b, we ablate three prototype selection strategies: segment-means, random, and greedy most-orthogonal selection. Segment-means, the strategy used in Nyströmformer, performs poorly

Table 5: **Comparison to the state-of-the-art on Long Range Arena benchmark.** GFLOPS and CUDA maximum Memory (MB) are reported for the ListOps task. Note that our algorithm achieves the best overall results with far fewer prototypes (64) than the other methods.

Model	ListOps	Text	Retrieval	Image	Pathfinder	Avg↑	GFLOPS↓	Mem.↓
Exact [76]	36.69	63.09	78.22	31.47	66.35	55.16	1.21	4579
Performer-256 [14]	36.69	63.22	78.98	29.39	66.55	54.97	0.49	885
Nystromformer-128 [85]	36.90	64.17	78.67	36.16	52.32	53.64	0.62	745
Orthoformer-64	33.87	64.42	78.36	33.26	66.41	55.26	0.24	344

Table 6: **Comparison to the state-of-the-art on video action recognition.** We report GFLOPS and top-1 (%) and top-5 (%) video action recognition accuracy on K-400/600, and SSv2. On Epic-Kitchens, we report top-1 (%) action (A), verb (V), and noun (N) accuracy.

(a) Something-Something V2					(b) Kinetics-400				
Model	Pretrain	Top-1	Top-5	GFLOPs × views	Method	Pretrain	Top-1	Top-5	GFLOPs × views
SlowFast [25]	K-400	61.7	-	$65.7 \times 3 \times 1$	I3D [10]	IN-1K	72.1	89.3	$108 \times N/A$
TSM [46]	K-400	63.4	88.5	$62.4 \times 3 \times 2$	R(2+1)D [75]	-	72.0	90.0	$152 \times 5 \times 23$
STM [33]	IN-1K	64.2	89.8	$66.5 \times 3 \times 10$	S3D-G [84]	IN-1K	74.7	93.4	$142.8 \times N/A$
MSNet [40]	IN-1K	64.7	89.4	$67 \times 1 \times 1$	X3D-XL [24]	-	79.1	93.9	$48.4 \times 3 \times 10$
TEA [45]	IN-1K	65.1	-	$70 \times 3 \times 10$	SlowFast [25]	-	79.8	93.9	$234 \times 3 \times 10$
bLVNet [23]	IN-1K	65.2	90.3	$128.6 \times 3 \times 10$	VTN [51]	IN-21K	78.6	93.7	$4218 \times 1 \times 1$
VidTr-L [44]	IN-21K+K-400	60.2	-	$351 \times 3 \times 10$	VidTr-L [44]	IN-21K	79.1	93.9	$392 \times 3 \times 10$
Tformer-L [7]	IN-21K	62.5	-	$1703 \times 3 \times 1$	Tformer-L [7]	IN-21K	80.7	94.7	$2380 \times 3 \times 1$
ViViT-L [2]	IN-21K+K-400	65.4	89.8	$3992 \times 4 \times 3$	MViT-B [22]	-	81.2	95.1	$455 \times 3 \times 3$
MViT-B [22]	K-400	67.1	90.8	$170 \times 3 \times 1$	ViViT-L [2]	IN-21K	81.3	94.7	$3992 \times 3 \times 4$
Mformer	IN-21K+K-400	66.5	90.1	$369.5 \times 3 \times 1$	Mformer	IN-21K	79.7	94.2	$369.5 \times 3 \times 10$
Mformer-L	IN-21K+K-400	68.1	91.2	$1185.1 \times 3 \times 1$	Mformer-L	IN-21K	80.2	94.8	$1185.1 \times 3 \times 10$
Mformer-HR	IN-21K+K-400	67.1	90.6	$958.8 \times 3 \times 1$	Mformer-HR	IN-21K	81.1	95.2	$958.8 \times 3 \times 10$

(c) Epic-Kitchens					(d) Kinetics-600				
Method	Pretrain	A	V	N	Model	Pretrain	Top-1	Top-5	GFLOPs × views
TSN [78]	IN-1K	33.2	60.2	46.0	AttnNAS [81]	-	79.8	94.4	-
TRN [86]	IN-1K	35.3	65.9	45.4	LGD-3D [56]	IN-1K	81.5	95.6	-
TBN [36]	IN-1K	36.7	66.0	47.2	SlowFast [25]	-	81.8	95.1	$234 \times 3 \times 10$
TSM [46]	IN-1K	38.3	67.9	49.0	X3D-XL [24]	-	81.9	95.5	$48.4 \times 3 \times 10$
SlowFast [25]	K-400	38.5	65.6	50.0	Tformer-HR [7]	IN-21K	82.4	96.0	$1703 \times 3 \times 1$
ViViT-L [2]	IN-21K+K-400	44.0	66.4	56.8	ViViT-L [2]	IN-21K	83.0	95.7	$3992 \times 3 \times 4$
Mformer	IN-21K+K-400	43.1	66.7	56.5	MViT-B-24 [22]	-	83.8	96.3	$236 \times 1 \times 5$
Mformer-L	IN-21K+K-400	44.1	67.1	57.6	Mformer	IN-21K	81.6	95.6	$369.5 \times 3 \times 10$
Mformer-HR	IN-21K+K-400	44.5	67.0	58.5	Mformer-L	IN-21K	82.2	96.0	$1185.1 \times 3 \times 10$
					Mformer-HR	IN-21K	82.7	96.1	$958.8 \times 3 \times 10$

because it can generate multiple parallel prototypes, which will over-estimate the relative probability of query–key pairs near those redundant prototypes. In contrast, our proposed strategy of selecting the most orthogonal prototypes from the query and key set works the best across both datasets, because it explicitly minimises prototype redundancy with respect to direction.

Number of prototypes. In Table 3c, we show that Orthoformer improves monotonically as the number of prototypes is increased. In particular, we see an average performance improvement of 4% on both datasets as we increase the number of prototypes from 16 to 128.

Temporally-shared prototypes. In Table 3d, we demonstrate the memory savings and performance benefits of sharing prototypes across time. On SSv2, we observe a 2% improvement in performance and a 5× decrease in memory usage. These gains may be attributed to the regularization effect of having prototypes leverage redundant information across frames.

4.3 Comparison to the state-of-the-art

In Table 6, we compare our method against the current state-of-the-art on four common benchmarking datasets: Kinetics-400, Kinetics-600, Something–Something v2 and Epic-Kitchens. We find that our method performs favorably against current methods, even when compared against much larger models

such as ViViT-L. In particular, it achieves strong top-1 accuracy improvements of 1.0% and 2.3% for SSv2 and Epic-Kitchen Nouns, respectively. These datasets require greater motion reasoning than Kinetics and so are a more challenging benchmark for video action recognition.

5 Conclusion

We have presented a new general-purpose attention block for video data that aggregates information along implicitly determined motion trajectories, lending a realistic inductive bias to the model. We further address its quadratic dependence on the input size with a new attention approximation algorithm that significantly reduces the memory requirements, the largest bottleneck for transformer models. With these contributions, we obtain state-of-the-art results on several benchmark datasets. Nonetheless, our approach inherits many of the limitations of transformer models, including poor data efficiency and slow training. Specific to this work, trajectory attention has higher computational complexity than alternative attention operations used for video data. This is attenuated by the proposed approximation algorithm, with significantly reduced memory and computation requirements. However, its runtime is bottlenecked by prototype selection, which is not easily parallelized.

Potential negative societal impacts. One negative impact of this research is the significant environmental impact associated with training transformers, which are large and compute-expensive models. Compared to 3D-CNNs where the compute scales linearly with the sequence length, video transformers scale quadratically. To mitigate this, we proposed an approximation algorithm with linear complexity that greatly reduces the computational requirements. There is also potential for video action recognition models to be misused, such as for unauthorized surveillance.

Acknowledgments and Disclosure of Funding

We are grateful for support from the Rhodes Trust (M.P.), Qualcomm Innovation Fellowship (Y.A.), the Royal Academy of Engineering (DFR05420, J.H), and EPSRC Centre for Doctoral Training in Autonomous Intelligent Machines & Systems [EP/L015897/1] (M.P. and Y.A.). M.P. funding was received under his Oxford affiliation. We thank Bernie Huang, Dong Guo, Rose Kanjirathinkal, Gedas Bertasius, Mike Zheng Shou, Mathilde Caron, Hugo Touvron, Benjamin Lefauze, Haoqi Fan, and Geoffrey Zweig from Facebook AI for their help, support, and discussion around this project. We also thank Max Bain and Tengda Han from VGG for fruitful discussions.

References

- [1] Hassan Akbari, Linagzhe Yuan, Rui Qian, Wei-Hong Chuang, Shih-Fu Chang, Yin Cui, and Boqing Gong. Vatt: Transformers for multimodal self-supervised learning from raw video, audio and text, 2021.
- [2] Anurag Arnab, Mostafa Dehghani, Georg Heigold, Chen Sun, Mario Lučić, and Cordelia Schmid. Vivit: A video vision transformer, 2021.
- [3] Jimmy Lei Ba, Jamie Ryan Kiros, and Geoffrey E. Hinton. Layer normalization, 2016.
- [4] Alexei Baevski, Yuhao Zhou, Abdelrahman Mohamed, and Michael Auli. wav2vec 2.0: A framework for self-supervised learning of speech representations. In *NeurIPS*, 2020.
- [5] Max Bain, Arsha Nagrani, Gü̈l Varol, and Andrew Zisserman. Frozen in time: A joint video and image encoder for end-to-end retrieval, 2021.
- [6] Iz Beltagy, Matthew E. Peters, and Arman Cohan. Longformer: The long-document transformer. 2020.
- [7] Gedas Bertasius, Heng Wang, and Lorenzo Torresani. Is space-time attention all you need for video understanding? In *ICML*, 2021.
- [8] Tom Brown, Benjamin Mann, Nick Ryder, Melanie Subbiah, Jared D Kaplan, Prafulla Dhariwal, Arvind Neelakantan, Pranav Shyam, Girish Sastry, Amanda Askell, Sandhini Agarwal, Ariel Herbert-Voss, Gretchen Krueger, Tom Henighan, Rewon Child, Aditya Ramesh, Daniel Ziegler, Jeffrey Wu, Clemens Winter, Chris Hesse, Mark Chen, Eric Sigler, Mateusz Litwin, Scott Gray, Benjamin Chess, Jack Clark, Christopher Berner, Sam McCandlish, Alec Radford, Ilya Sutskever, and Dario Amodei. Language models are few-shot learners. In *NeurIPS*, 2020.
- [9] Nicolas Carion, Francisco Massa, Gabriel Synnaeve, Nicolas Usunier, Alexander Kirillov, and Sergey Zagoruyko. End-to-end object detection with transformers. In *ECCV*, 2020.
- [10] Joao Carreira and Andrew Zisserman. Quo vadis, action recognition? a new model and the kinetics dataset. In *CVPR*, 2017.
- [11] Mark Chen, Alec Radford, Rewon Child, Jeff Wu, Heewoo Jun, Prafulla Dhariwal, David Luan, and Ilya Sutskever. Generative pretraining from pixels. In *ICML*, 2020.
- [12] Yunpeng Chen, Yannis Kalantidis, Jianshu Li, Shuicheng Yan, and Jiashi Feng. a^2 -nets: Double attention networks. In *NeurIPS*, 2018.
- [13] Rewon Child, Scott Gray, Alec Radford, and Ilya Sutskever. Generating long sequences with sparse transformers. URL <https://openai.com/blog/sparse-transformers>, 2019.
- [14] Krzysztof Marcin Choromanski, Valerii Likhoshesterov, David Dohan, Xingyou Song, Andreea Gane, Tamas Sarlos, Peter Hawkins, Jared Quincy Davis, Afroz Mohiuddin, Lukasz Kaiser, David Benjamin Belanger, Lucy J Colwell, and Adrian Weller. Rethinking attention with performers. In *ICLR*, 2021.
- [15] E. Cubuk, Barret Zoph, Jonathon Shlens, and Quoc V. Le. Randaugment: Practical data augmentation with no separate search. In *CVPRW*, 2020.
- [16] Dima Damen, Hazel Doughty, Giovanni Maria Farinella, Antonino Furnari, Evangelos Kazakos, Jian Ma, Davide Moltisanti, Jonathan Munro, Toby Perrett, Will Price, et al. Rescaling egocentric vision. In *ECCV*, 2020.
- [17] Jia Deng, Wei Dong, Richard Socher, Li-Jia Li, Kai Li, and Li Fei-Fei. Imagenet: A large-scale hierarchical image database. In *CVPR*, 2009.
- [18] Karan Desai and Justin Johnson. VirTex: Learning Visual Representations from Textual Annotations. In *CVPR*, 2021.
- [19] Carl Doersch, Ankush Gupta, and Andrew Zisserman. Crosstransformers: spatially-aware few-shot transfer. In *NeurIPS*, 2020.
- [20] Alexey Dosovitskiy, Lucas Beyer, Alexander Kolesnikov, Dirk Weissenborn, Xiaohua Zhai, Thomas Unterthiner, Mostafa Dehghani, Matthias Minderer, Georg Heigold, Sylvain Gelly, Jakob Uszkoreit, and Neil Houlsby. An image is worth 16x16 words: Transformers for image recognition at scale. In *ICLR*, 2021.
- [21] Haoqi Fan, Yanghao Li, Bo Xiong, Wan-Yen Lo, and Christoph Feichtenhofer. Pyslowfast. <https://github.com/facebookresearch/slowfast>, 2020.
- [22] Haoqi Fan, Bo Xiong, Karttikeya Mangalam, Yanghao Li, Zhicheng Yan, Jitendra Malik, and Christoph Feichtenhofer. Multiscale vision transformers, 2021.
- [23] Quanfu Fan, Chun-Fu (Ricarhd) Chen, Hilde Kuehne, Marco Pistoia, and David Cox. More Is Less: Learning Efficient Video Representations by Temporal Aggregation Modules. In *NeurIPS*, 2019.
- [24] Christoph Feichtenhofer. X3d: Expanding architectures for efficient video recognition. In *CVPR*, 2020.
- [25] Christoph Feichtenhofer, Haoqi Fan, Jitendra Malik, and Kaiming He. Slowfast networks for video recognition. In *ICCV*, 2019.
- [26] Valentin Gabeur, Chen Sun, Karteek Alahari, and Cordelia Schmid. Multi-modal transformer for video retrieval. In *ECCV*, 2020.
- [27] Raghav Goyal, Samira Ebrahimi Kahou, Vincent Michalski, Joanna Materzynska, Susanne Westphal, Heuna Kim, Valentin Haenel, Ingo Fruend, Peter Yianilos, Moritz Mueller-Freitag, and et al. The “something something” video database for learning and evaluating visual common sense. In *ICCV*, 2017.
- [28] Kaiming He, Xiangyu Zhang, Shaoqing Ren, and Jian Sun. Deep residual learning for image recognition. In *CVPR*, 2016.
- [29] Po-Yao Huang, Mandela Patrick, Junjie Hu, Graham Neubig, Florian Metze, and Alexander Hauptmann. Multilingual multimodal pre-training for zero-shot cross-lingual transfer of vision-language models. In *NAACL*, 2021.

[30] Eddy Ilg, Nikolaus Mayer, Tonmoy Saikia, Margret Keuper, Alexey Dosovitskiy, and Thomas Brox. Flownet 2.0: Evolution of optical flow estimation with deep networks. In *CVPR*, 2016.

[31] Allan Jabri, Andrew Owens, and Alexei Efros. Space-time correspondence as a contrastive random walk. In *NeurIPS*, 2020.

[32] Kenton Lee Jacob Devlin, Ming-Wei Chang and Kristina Toutanova. BERT: Pre-training of deep bidirectional transformers for language understanding. In *NAACL*, 2018.

[33] Boyuan Jiang, Mengmeng Wang, Weihao Gan, Wei Wu, and Junjie Yan. Stm: Spatiotemporal and motion encoding for action recognition. In *ICCV*, 2019.

[34] Shihao Jiang, Dylan Campbell, Yao Lu, Hongdong Li, and Richard Hartley. Learning to estimate hidden motions with global motion aggregation, 2021.

[35] Will Kay, Joao Carreira, Karen Simonyan, Brian Zhang, Chloe Hillier, Sudheendra Vijayanarasimhan, Fabio Viola, Tim Green, Trevor Back, Paul Natsev, et al. The kinetics human action video dataset, 2017.

[36] Evangelos Kazakos, Arsha Nagrani, Andrew Zisserman, and Dima Damen. Epic-fusion: Audio-visual temporal binding for egocentric action recognition. In *ICCV*, 2019.

[37] Nikita Kitaev, Lukasz Kaiser, and Anselm Levskaya. Reformer: The efficient transformer. In *ICLR*, 2020.

[38] Alexander Klaser, Marcin Marszałek, and Cordelia Schmid. A spatio-temporal descriptor based on 3d-gradients. In *BMVC*, 2008.

[39] Alex Krizhevsky, Ilya Sutskever, and Geoffrey E. Hinton. Imagenet classification with deep convolutional neural networks. In *NeurIPS*, 2012.

[40] Heeseung Kwon, Manjin Kim, Suha Kwak, and Minsu Cho. Motionsqueeze: Neural motion feature learning for video understanding. In *ECCV*, 2020.

[41] Yann LeCun, Léon Bottou, Yoshua Bengio, and Patrick Haffner. Gradient-based learning applied to document recognition. *Proceedings of the IEEE*, 86(11):2278–2324, 1998.

[42] Sangho Lee, Youngjae Yu, Gunhee Kim, Thomas Breuel, Jan Kautz, and Yale Song. Parameter efficient multimodal transformers for video representation learning. In *ICLR*, 2021.

[43] Liunian Harold Li, Mark Yatskar, Da Yin, Cho-Jui Hsieh, and Kai-Wei Chang. Visualbert: A simple and performant baseline for vision and language, 2019.

[44] Xinyu Li, Yanyi Zhang, Chunhui Liu, Bing Shuai, Yi Zhu, Biagio Brattoli, Hao Chen, Ivan Marsic, and Joseph Tighe. Vidtr: Video transformer without convolutions, 2021.

[45] Yan Li, Bin Ji, Xintian Shi, Jianguo Zhang, Bin Kang, and Limin Wang. Tea: Temporal excitation and aggregation for action recognition. In *CVPR*, 2020.

[46] Ji Lin, Chuang Gan, and Song Han. Tsm: Temporal shift module for efficient video understanding. 2019.

[47] Francesco Locatello, Dirk Weissenborn, Thomas Unterthiner, Aravindh Mahendran, Georg Heigold, Jakob Uszkoreit, Alexey Dosovitskiy, and Thomas Kipf. Object-centric learning with slot attention. In *NeurIPS*, 2020.

[48] Ilya Loshchilov and Frank Hutter. Fixing weight decay regularization in adam, 2018.

[49] Jiasen Lu, Dhruv Batra, Devi Parikh, and Stefan Lee. Vibert: Pretraining task-agnostic visiolinguistic representations for vision-and-language tasks. In *NeurIPS*, 2019.

[50] Paulius Micikevicius, Sharan Narang, Jonah Alben, Gregory Diamos, Erich Elsen, David Garcia, Boris Ginsburg, Michael Houston, Oleksii Kuchaiev, Ganesh Venkatesh, and Hao Wu. Mixed precision training. In *ICLR*, 2018.

[51] Daniel Neiman, Omri Bar, Maya Zohar, and Dotan Asselmann. Video transformer network, 2021.

[52] Niki Parmar, Ashish Vaswani, Jakob Uszkoreit, Łukasz Kaiser, Noam Shazeer, Alexander Ku, and Dustin Tran. Image transformer. In *ICML*, 2018.

[53] Mandela Patrick, Yuki M. Asano, Bernie Huang, Ishan Misra, Florian Metze, Joao Henriques, and Andrea Vedaldi. Space-time crop & attend: Improving cross-modal video representation learning, 2021.

[54] Mandela Patrick, Po-Yao Huang, Yuki Asano, Florian Metze, Alexander G Hauptmann, Joao F. Henriques, and Andrea Vedaldi. Support-set bottlenecks for video-text representation learning. In *ICLR*, 2021.

[55] Zhaofan Qiu, Ting Yao, and Tao Mei. Learning spatio-temporal representation with pseudo-3d residual networks. In *ICCV*, 2017.

[56] Zhaofan Qiu, Ting Yao, Chong-Wah Ngo, Xinmei Tian, and Tao Mei. Learning spatio-temporal representation with local and global diffusion. *CVPR*, 2019.

[57] Alec Radford, Jeffrey Wu, Rewon Child, David Luan, Dario Amodei, and Ilya Sutskever. Language models are unsupervised multitask learners. *OpenAI Blog*, 1(8):9, 2019.

[58] Deva Ramanan, David A. Forsyth, and Andrew Zisserman. Strike a pose: Tracking people by finding stylized poses. In *Proc. CVPR*, 2005.

[59] Olga Russakovsky, Jia Deng, Hao Su, Jonathan Krause, Sanjeev Satheesh, Sean Ma, Zhiheng Huang, Andrej Karpathy, Aditya Khosla, Michael Bernstein, Alexander C. Berg, and Li Fei-Fei. ImageNet Large Scale Visual Recognition Challenge. *IJCV*, 2015.

[60] Mert Bulent Sarıyıldız, Julien Perez, and Diane Larlus. Learning visual representations with caption annotations. In *ECCV*, 2020.

[61] P. Scovanner, S. Ali, and M. Shah. A 3-dimensional sift descriptor and its application to action recognition. In *ACM MM*, 2007.

[62] Michael C Shewry and Henry P Wynn. Maximum entropy sampling. *Journal of Applied Statistics*, 14(2):165–170, 1987.

[63] Weijie Su, Xizhou Zhu, Yue Cao, Bin Li, Lewei Lu, Furu Wei, and Jifeng Dai. Vi-bert: Pre-training of generic visual-linguistic representations. In *ICLR*, 2020.

[64] Chen Sun, Fabien Baradel, Kevin Murphy, and Cordelia Schmid. Contrastive bidirectional transformer for temporal representation learning, 2019.

[65] Chen Sun, Austin Myers, Carl Vondrick, Kevin Murphy, and Cordelia Schmid. Videobert: A joint model for video and language representation learning. In *ICCV*, 2019.

[66] Deqing Sun, Xiaodong Yang, Ming-Yu Liu, and Jan Kautz. Pwc-net: Cnns for optical flow using pyramid, warping, and cost volume. In *CVPR*, 2018.

[67] Christian Szegedy, Vincent Vanhoucke, Sergey Ioffe, Jonathon Shlens, and Zbigniew Wojna. Rethinking the inception architecture for computer vision. In *CVPR*, 2016.

[68] Hao Tan and Mohit Bansal. Lxmert: Learning cross-modality encoder representations from transformers. In *EMNLP*, 2019.

[69] Hao Tan and Mohit Bansal. Vokenization: Improving language understanding with contextualized, visual-grounded supervision. In *EMNLP*, 2020.

[70] Yi Tay, Mostafa Dehghani, Samira Abnar, Yikang Shen, Dara Bahri, Philip Pham, Jinfeng Rao, Liu Yang, Sebastian Ruder, and Donald Metzler. Long range arena : A benchmark for efficient transformers. In *ICLR*, 2021.

[71] Zachary Teed and Jia Deng. RAFT: recurrent all-pairs field transforms for optical flow. In *Proc. ECCV*, 2020.

[72] Hugo Touvron, Matthieu Cord, Matthijs Douze, Francisco Massa, Alexandre Sablayrolles, and Hervé Jégou. Training data-efficient image transformers & distillation through attention. In *ICML*, 2021.

[73] Du Tran, Lubomir Bourdev, Rob Fergus, Lorenzo Torresani, and Manohar Paluri. Learning spatiotemporal features with 3d convolutional networks. In *ICCV*, 2015.

[74] Du Tran, Heng Wang, Matt Feiszli, and Lorenzo Torresani. Video classification with channel-separated convolutional networks. In *ICCV*, 2019.

[75] Du Tran, Heng Wang, Lorenzo Torresani, Jamie Ray, Yann LeCun, and Manohar Paluri. A closer look at spatiotemporal convolutions for action recognition. In *CVPR*, 2018.

[76] Ashish Vaswani, Noam Shazeer, Niki Parmar, Jakob Uszkoreit, Llion Jones, Aidan N. Gomez, Łukasz Kaiser, and Illia Polosukhin. Attention is all you need. In *NIPS*, 2017.

[77] Heng Wang and Cordelia Schmid. Action recognition with improved trajectories. In *ICCV*, 2013.

[78] Limin Wang, Yuanjun Xiong, Yu Qiao, Dahua Lin, Xiaoou Tang, and Luc Van Gool. Temporal segment networks: Towards good practices for deep action recognition. In *ECCV*, 2016.

[79] Sinong Wang, Belinda Li, Madian Khabsa, Han Fang, and Hao Ma. Linformer: Self-attention with linear complexity. In *NeurIPS*, 2020.

[80] Xiaolong Wang, Ross Girshick, Abhinav Gupta, and Kaiming He. Non-local neural networks. In *CVPR*, 2018.

[81] Xiaofang Wang, Xuehan Xiong, Maxim Neumann, AJ Piergiovanni, Michael S Ryoo, Anelia Angelova, Kris M Kitani, and Wei Hua. Attentionnas: Spatiotemporal attention cell search for video classification. In *ECCV*, 2020.

[82] Ross Wightman. Pytorch image models. <https://github.com/rwightman/pytorch-image-models>, 2019.

[83] Bichen Wu, Chenfeng Xu, Xiaoliang Dai, Alvin Wan, Peizhao Zhang, Masayoshi Tomizuka, Kurt Keutzer, and Peter Vajda. Visual transformers: Token-based image representation and processing for computer vision, 2020.

[84] Saining Xie, Chen Sun, Jonathan Huang, Zhuowen Tu, and Kevin Murphy. Rethinking spatiotemporal feature learning: Speed-accuracy trade-offs in video classification. In *ECCV*, 2018.

[85] Yunyang Xiong, Zhanpeng Zeng, Rudrasis Chakraborty, Mingxing Tan, Glenn Fung, Yin Li, and Vikas Singh. Nyströmformer: A nyström-based algorithm for approximating self-attention. In *AAAI*, 2021.

[86] Bolei Zhou, Alex Andonian, Aude Oliva, and Antonio Torralba. Temporal relational reasoning in videos. In *ECCV*, 2018.

[87] Linchao Zhu and Yi Yang. Actbert: Learning global-local video-text representations. In *CVPR*, 2020.

6 Appendix

6.1 Further experimental analysis and results

6.1.1 Does trajectory attention make better use of motion cues?

In the main paper (and below in Section 6.1.2), we provide evidence that action classification on the Something-Something V2 (SSv2) dataset [27] is more reliant on motion cues than the Kinetics dataset [35], where appearance cues dominate and a single-frame model achieves high accuracy. Improved performance on SSV2 is one way to infer that our model makes better use of temporal information, however, here we consider another way. We artificially adjust the speed of the video clips by changing the temporal stride of the input. A larger stride simulates faster motions, with adjacent frames being more different. If our trajectory attention is able to make better use of the temporal information in the video than the other attention mechanisms, we expect the margin of improvement to increase as the temporal stride increases. As shown in Figure 3, this is indeed what we observe, with the lines diverging as temporal stride increases, especially for the motion cue-reliant SSV2 dataset. Since the same number of frames are used as input in all cases, the larger the stride, the more of the video clip is seen by the model. This provides additional confirmation that seeing a small part of a Kinetics video is usually enough to classify it accurately, as shown on the bottom left, where the absolute accuracy is reported.

6.1.2 How important are motion cues for classifying videos from the Kinetics-400 and Something-Something V2 datasets?

To determine the relative importance of motion cues compared to appearance cues for classifying videos on two of the major video action recognition datasets (Kinetics-400 and Something-Something V2), we trained a single frame vision transformer model and compare the results to a multi-frame model that can reason about motion. The single frame was sampled from the video at random. Table 7 shows that single-frame action classifiers can do almost as well as video action classifiers on the Kinetics-400 dataset, implying that the motion information is much less relevant. In contrast, classifying videos from the Something-Something V2 dataset clearly requires this motion information. Therefore, to excel on the SSV2 dataset, a model must reason about motion information. Our model, which introduces an inductive bias that favors pooling along motion trajectories, is able to do this and sees corresponding performance gains.

Table 7: **Importance of motion cues for the K-400 and SSV2 datasets.** A classifier for the K-400 dataset performs well when all motion information is removed (1 frame model), while a classifier for the SSV2 dataset performs very poorly. Therefore, SSV2 is a better dataset for evaluating *video* action classification, where the combination of appearance and motion is critical.

Dataset	Top-1 accuracy (1 frame)	Top-1 accuracy (8 frames)	Δ
Kinetics-400	73.2	79.7	6.5
Something-Something V2	27.1	66.5	39.4

6.1.3 Can we train larger models using approximated trajectory attention?

The Orthoformer attention approximation algorithm allows us to train larger models and higher resolution inputs for a given GPU memory budget. Here, we verify that this is the case, by training a large vision transformer model (ViT-L/16) [20] with a higher resolution input (336×336 pixels) on the Kinetics-400 dataset, using the Orthoformer approximation with 196 temporally-shared prototypes and the same schedule as the base model. We use a fixed patch size (in pixels) for all models, and so the number of input tokens to the transformer scales with the square of the image resolution. As shown in Table 8, this model achieves a competitive accuracy without fine-tuning the training schedule, hyperparameters or data augmentation strategy. We expect that fine-tuning these on a validation set would greatly improve the model’s performance, based on results from contemporary work [2]. Obviously such a parameter sweep is more time-consuming for these large models than the base model, however these preliminary results are indicative that higher accuracies are attainable if these parameters were to be optimized.

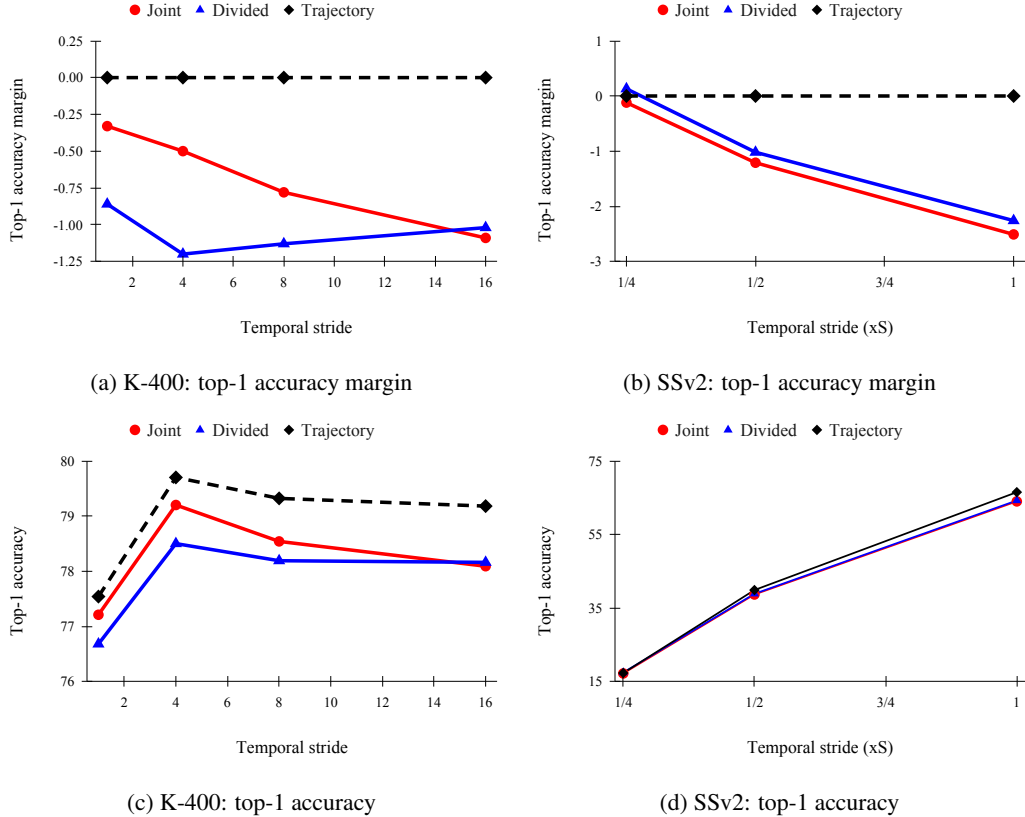


Figure 3: **Does trajectory attention make better use of motion cues?** Performance of transformer models with joint space-time attention, divided space-time attention, and trajectory attention, as the temporal stride increases, on the Kinetics-400 dataset (left) and the Something-Something V2 dataset (right). Top: top-1 accuracy margin relative to trajectory attention (difference of accuracy and trajectory accuracy). Bottom: absolute top-1 accuracy shown for reference. If our trajectory attention is able to make better use of the temporal information in the video than the other attention mechanisms, we expect the accuracy margin between the methods to increase as the temporal stride increases. This is indeed the observed behaviour, especially for the motion cue-reliant SSv2 dataset. A larger stride simulates greater motion between input frames, which trajectory attention is better able to model and reason about. Note that the larger the stride, the more of the video clip is seen by the model; for all plots, the rightmost side of the axis corresponds to the entire video clip. Note also that the strides for SSv2 are written as multiples of S , the stride needed to evenly sample the entire video clip.

6.1.4 Trajectory attention maps

In Figure 4, we show qualitative results of the intermediate attention maps of our trajectory attention operation. The learned attention maps appear to implicitly track the query points across time, a strategy that is easier to learn with the inductive bias instilled by trajectory attention.

6.2 Implementation details

Preprocessing. During training, we randomly sample clips of size $16 \times 224 \times 224$ at a rate of $1/4$ from 30 FPS videos, thereby giving an effective temporal resolution of just over 2 seconds. We normalize the inputs with mean and standard deviation 0.5, rescaling in the range $[-1, 1]$. We use standard video augmentations such as random scale jittering, random horizontal flips and color jittering. For smaller datasets such as Something-Something V2 and Epic-Kitchens, we additionally apply rand-augment [15]. During testing, we uniformly sample 10 clips per video and apply a 3 crop evaluation [25].

Table 8: **Can we train larger models using approximated trajectory attention?** We report top-1 and top-5 accuracy (%) on the Kinetics-400 dataset of two variants of our Motionformer model: Motionformer-B and Motionformer-H. The former uses the base model with exact (E) trajectory attention, while the latter uses a much larger model (ViT-L) and a higher resolution input (336×336 pixels) with approximate (A) trajectory attention, i.e., using Orthoformer. The larger model has better performance, despite no optimization of the training schedule, hyperparameters, and data augmentation schedule. The larger model also has far more parameters than the base model, and so unavoidably requires more GPU memory. Furthermore, for a fixed patch size (in pixels), the memory requirements for exact attention scale with the square of the input resolution. We reduce this to a linear relationship with the Orthoformer approximation, which allows us to fit the model on the GPU.

Model	Base model	Params	Attention	Max memory (GB)	Top-1	Top-5
Mformer-B	ViT-B/224	109.1M	Trajectory (E)	7.3	79.7	94.2
Mformer-H	ViT-L/336	381.9M	Trajectory (A)	22.2	80.0	94.5

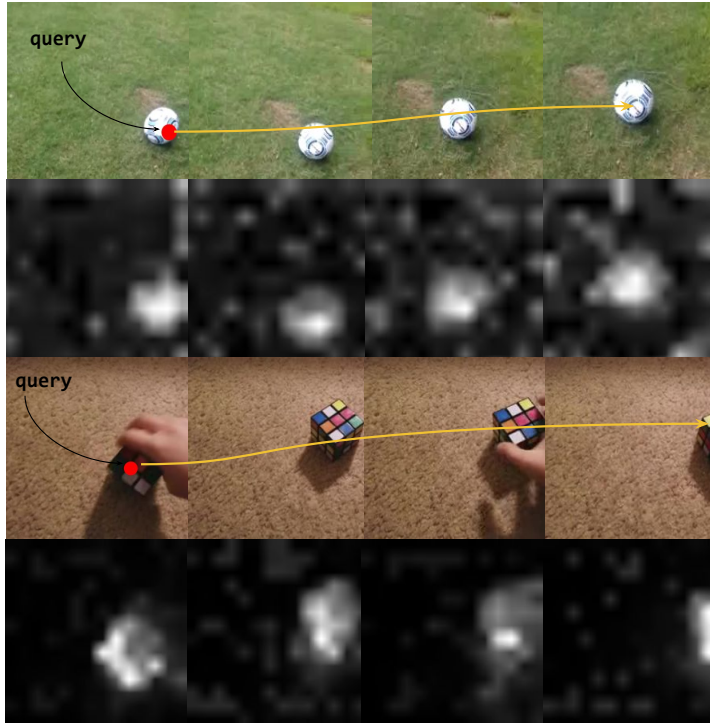


Figure 4: **Trajectory attention maps.** In this sequence of frames from Kinetics-400 (row 1) and Something-Something V2 (row 3), we show the attention maps at each frame given an initial query point (red point). We see that the model learns to implicitly track along motion paths (yellow arrow) using our trajectory attention module.

Training. For all datasets, we use the AdamW [48] optimizer with weight decay 5×10^{-2} , a batch size per GPU of 4, label smoothing [67] with alpha 0.2 and mixed precision training [50]. For Kinetics-400/600 and Something-Something V2, we train for 35 epochs, with an initial learning rate of 10^{-4} , which we decay by 10 at epochs 20, 30. As Epic-Kitchens is a smaller dataset, we use a longer schedule and train for 50 epochs with decay at 30 and 40.

Long Range Arena benchmark details. For the Long-Range Arena benchmark [70], we used the training, validation, and testing code and parameters from the Nyströmformer Github repository. The Performer [14] implementation was ported over to PyTorch from the official Github repo, and the Nyströmformer [85] implementation was used directly from its Github repository.

Computing resources. Ablation experiments were run on a GPU cluster using 4 nodes (32 GPUs) with an average training time of 12 hours. Experiments for comparing with state-of-the-art models used 8 nodes (64 GPUs), with an average training time of 7 hours.

Libraries. For our code implementation, we used the `timm` [82] library for our base vision transformer implementation, and the `PySlowFast` [21] library for training, data processing, and the evaluation pipeline.